

Towards Efficient Scene Understanding via Squeeze Reasoning

Xiangtai Li¹, Xia Li¹, Ansheng You¹, Li Zhang², Guangliang Cheng⁴, Kuiyuan Yang³, Yunhai Tong¹, Zhouchen Lin¹

¹School of EECS, Peking University ²University of Oxford ³DeepMotion ⁴SenseTime Research
 {lxtpk, ethanlee, youansheng, yhtong, zlin}@pku.edu.cn
 lz@robots.ox.ac.uk, chengguangliang@sensetime.com, kuiyuanyang@deepmotion.ai

Abstract

Graph-based convolutional model such as non-local block has shown to be effective for strengthening the context modeling ability in convolutional neural networks (CNNs). However, its pixel-wise computational overhead is prohibitive which renders it unsuitable for high resolution imagery. In this paper, we explore the efficiency of context graph reasoning and propose a novel framework called Squeeze Reasoning. Instead of propagating information on the spatial map, we first learn to squeeze the input feature into a channel-wise global vector and perform reasoning within the single vector where the computation cost can be significantly reduced. Specifically, we build the node graph in the vector where each node represents an abstract semantic concept. The refined feature within the same semantic category results to be consistent, which is thus beneficial for downstream tasks. We show that our approach can be modularized as an end-to-end trained block and can be easily plugged into existing networks. Despite its simplicity and being lightweight, our strategy allows us to establish a new state-of-the-art on semantic segmentation and show significant improvements with respect to strong, state-of-the-art baselines on various other scene understanding tasks including object detection, instance segmentation and panoptic segmentation. Code will be made available to foster any further research¹.

Introduction

Convolutional neural networks have proven to be effective and useful to learn visual representations in an end-to-end fashion with a certain objective task such as, semantic segmentation (Long, Shelhamer, and Darrell 2015), image classification (He et al. 2016), object detection (Ren et al. 2015), instance segmentation (He et al. 2017) and panoptic segmentation (Kirillov et al. 2019b). However, the effective receptive field (Luo et al. 2016) of CNNs grows slowly if we simply stacking local convolutional layers. Thus, the limited receptive field prevents the model from taking all the contextual information into account and thus renders the model insufficiently covering all the regions of interest.

A broad range of prior research has investigated network architecture designs to increase the receptive field-of-view such as self-attention/Non-local (Wang et al. 2018b), channel attention (Hu, Shen, and Sun 2018), and graph convolution network (GCN) (Chen et al. 2019). Although they have

¹Code request email: lxtpk@pku.edu.cn

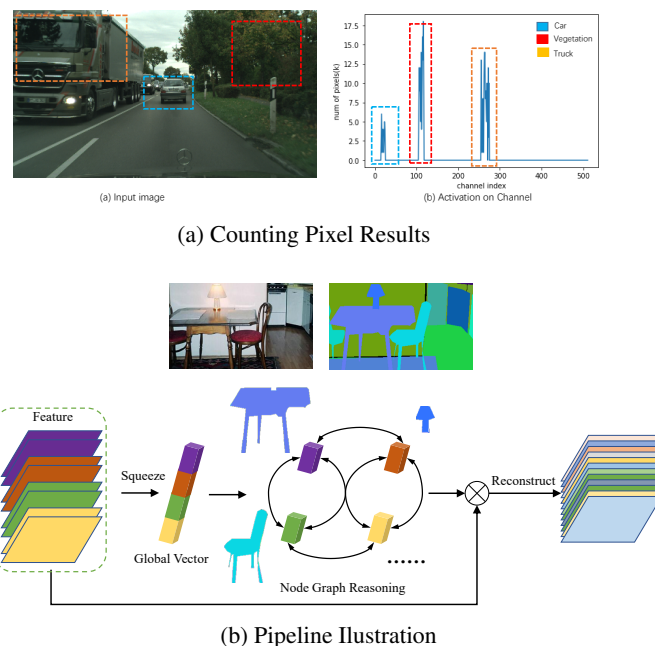


Figure 1: (a) Toy Experiment results by counting pixels given specific classes using trained model. (b) Illustration of our proposed module for semantic segmentation task. Best view in color and zoom in.

been shown to be effective in strengthening the representations produced by CNNs, modeling the inter-dependencies in a high-dimensional space prevents them from fully exploiting the sparse property required by the final classifier. Furthermore, they suffer from the prohibitively expensive computation overhead during training and inference, *e.g.*, the large affinity matrix at each spatial position (Hu, Shen, and Sun 2018) or channel position (Chen et al. 2019), which renders these methods unsuitable for high-resolution inputs. Although recent methods reduce such cost by involving fewer pixels (Huang et al. 2018b) or selecting representative nodes (Zhu et al. 2019b), their computation is still huge given high resolution image inputs.

Could we find another way to eliminate the limitation of high-cost spatial information while capturing global context

information? We first carry out toy experiments using a pre-trained Deeplabv3+ model (Chen et al. 2018a). We count the pixels on the final normalized feature (512 dimensions before classification) given ground truth masks whose activation values are beyond 0.8. As shown in Fig 1(a), we find different classes lie in different groups along channels sparsely. We only show three classes for simplicity. This motivates us to build an information propagation module on channel solely where each group represents one specific semantic class while the cost of spatial resolution can be avoided. Inspired by SE-networks (Hu, Shen, and Sun 2018), we first squeeze the feature into a compact global vector and then perform reasoning operation on such compact vector. Benefit from squeezing, the computation cost can be significantly reduced compared with previous works. The schematic illustration of our proposed method is shown in Fig 1(b).

Our framework mainly contains three steps. First, we perform the node squeezing operation to obtain the global vector. This can be done by simply a global average pooling or using Hadamard product pooling to capture the second-order statistics. Then we carry out node reasoning by dividing such vector into different groups, and the inter-dependencies can be diffused through the reasoning process. Finally, we reconstruct the original feature map by multiplying the reasoned vector with the original input. Our approach can serve as a lightweight module and can be easily plugged into existing networks. Compare to Non-local (Wang et al. 2018b) or graph convolution network (Chen et al. 2019), which model the global relationship on feature spatial or channel dimension, our approach instead models the inter-dependencies on the squeezed global vector space, and notably, each node consists of a group of atom/channel. Therefore, our method uses substantially fewer floating-point operations and fewer parameters and memory costs. Moreover, our method achieves the best speed and accuracy trade-off on the Cityscapes test set, which shows its practical usage.

The contributions of this work are as follows: (i) We propose a novel squeeze reasoning framework for highly efficient deep feature representation learning for scene understanding tasks. (ii) An efficient node graph reasoning is introduced to model the inter-dependencies between abstract semantic nodes. This enables our method to serve as a lightweight and effective module and can be easily deployed in existing networks. (iii) Extensive experiments demonstrate that the proposed approach can establish new state-of-the-arts on four major semantic segmentation benchmark datasets including Cityscapes (Cordts et al. 2016), Pascal Context (Mottaghi et al. 2014), ADE20K (Zhou et al. 2016) while keeping efficiency, and show consistent improvement with respect to strong baselines on several scene understanding tasks with negligible cost.

Related work

Long-range modeling Beyond the standard convolutional operator used for short-range modeling, many long-range operators are proposed to aggregate information from large image regions, even the whole image. Global Average Pooling (GAP) (He et al. 2016), which bridges local feature maps

and global classifiers, is widely used for long-range modeling. In Squeeze-and-Excitation network (Hu, Shen, and Sun 2018), GAP is used in more intermediate layers for coupling global information and local information more thoroughly. In Pyramid Pooling Module (PPM) (Zhao et al. 2017), a pyramid of average pooling operators is used to harvest features. In addition to first-order statistics captured by GAP, bilinear pooling (Lin, RoyChowdhury, and Maji 2015) extracts image-level second-order statistics as complementary of convolutional features. Besides pooling-based operators, generalized convolutional operators (Bello et al. 2019) are also used for long-range modeling. Astrous convolution enlarges kernels by inserting zeros in between (Yu and Koltun 2016), which is further used by stacking kernels with multiple astrous rates pyramidally (Chen et al. 2015, 2018, 2017) or densely (Yang et al. 2018). Deformable convolution (Dai et al. 2017; Zhu et al. 2019a) generalizes atrous convolution by learning the offsets for convolution sampling locations. Non-local operator (Wang et al. 2018b) and its variants (Yue et al. 2018; Fu et al. 2018; He et al. 2019; Huang et al. 2018b) use self attention mechanism (Vaswani et al. 2017) to generalize GAP by weighing globally aggregation with pixel-to-pixel affinities.

Graph-based reasoning The graph removes the coordinate restriction of fixed spatial grids, where features organized in coordinate space are reorganized by nodes and linked by edges. EncNet (Zhang et al. 2018a) represents convolutional features on a set of nodes (visual centers) in a bag-of-word manner for global context modeling. In (Li and Gupta 2018; Liang et al. 2018; Chen et al. 2019), convolutional features are assigned to a set of nodes embedded in a latent space, and graph-based reasoning is further carried between these nodes for feature enhancement, then the enhanced features of each node are assigned back to coordinate space.

In our work, a global vector squeezed from the whole image is organized as a small graph for reasoning, where each node contains rich global information. Thus reasoning is carried on a high level, which is more efficient and robust to noises than previous methods.

Method

In this section, we first review related works (Hu, Shen, and Sun 2018; Kipf and Welling 2017; Wang et al. 2018b) as preliminary knowledge. Then detailed description and formulation of our SR module are introduced. Finally, we elaborate on how to apply it to several different computer vision tasks.

Preliminaries

Graph convolution. Assume an input matrix $\mathbf{X} \in \mathbb{R}^{D \times N}$, where D is the feature dimension and $N = H \times W$ is the number of locations defined on regular grid coordinates $\Omega = \{1, \dots, H\} \times \{1, \dots, W\}$. In standard convolution, information is only exchanged among positions in a small neighborhood defined by the filter size (typically 3×3). In order to create a large receptive field and capture long-range dependencies, one needs to stack numerous layers after each other, as done in common architectures (He et al. 2016).

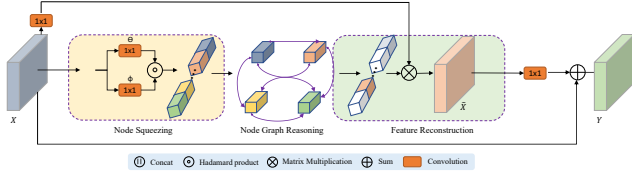


Figure 2: Schematic illustration of our proposed SR module. Our module contains three steps. Node Squeezing: squeeze the feature into separate nodes. Node Graph Reasoning: perform GCN reasoning in node space. Feature Reconstruction: reconstruct the feature by the reasoned global vector.

Graph convolution (Kipf and Welling 2017), is a highly efficient, effective and differentiable module that generalizes the neighborhood definition used in standard convolution and allows long-range information exchange in a single layer. This is done by defining edges \mathbb{E} among nodes \mathbb{V} in a graph \mathbb{G} . Formally, the graph convolution is defined as

$$\tilde{\mathbf{X}} = \sigma(\mathbf{W}\mathbf{X}\mathbf{A}), \quad (1)$$

where $\sigma(\cdot)$ is the non-linear activation function, $\mathbf{A} \in \mathbb{R}^{N \times N}$ is the adjacency matrix characterising the neighbourhood relations of the graph and $\mathbf{W} \in \mathbb{R}^{D \times \tilde{D}}$ is the weight matrix. So the graph definition and structure play a key role in determining the information propagation.

Non-local network. We describe non-local network (Wang et al. 2018b) in view of a fully connected graphical model. For a 2D input feature with the size of $C \times H \times W$, where C , H , and W denote the channel dimension, height, and width respectively, it can be interpreted as a set of features, $\mathbf{X} = [\mathbf{x}_1, \mathbf{x}_2, \dots, \mathbf{x}_N]^T$, $\mathbf{x}_i \in \mathbb{R}^C$, where N is the number of nodes (e.g. $N = H \times W$), and C is the node feature dimension.

$$\tilde{\mathbf{X}} = \delta(\mathbf{X}_\theta \mathbf{X}_\phi^T) \mathbf{X}_g = \mathbf{A}(\mathbf{X}) \mathbf{X}_g, \quad (2)$$

where $\mathbf{A}(\mathbf{X}) \in \mathbb{R}^{N \times N}$ indicates the affinity matrix, $\mathbf{X}_\theta \in \mathbb{R}^{N \times C'}$, $\mathbf{X}_\phi \in \mathbb{R}^{N \times C'}$, and $\mathbf{X}_g \in \mathbb{R}^{N \times C'}$ which are projection matrix. In summary, according to Equ. 1 and Equ. 2 both the computation and affinity cost are highly dependent on the number of node N .

‘Squeeze’ operation. The ‘squeeze’ operation is commonly used in networks for image classification, and adopted in SE-net (Hu, Shen, and Sun 2018) to summarize the global contexts for intermediate layers for channel weights recalibration. One simple implementation of this operation is the Global Average Pooling (GAP).

SR module formulation

As discussed, pixels or nodes’ choices are essential for reducing computation cost for both graph convolution models and non-local models. Recent works (Huang et al. 2018b; Yuan, Chen, and Wang 2020) follow this idea to achieve less computation cost. However, both the affinity memory and computation cost are still linearly dependent on the input resolution. In particular, this will limit their usage for some applications such as road scene understanding with high-resolution image inputs. Different from their approaches, we

propose a simple yet effective framework named Squeeze Reasoning. Our approach mainly contains three steps. First, we squeeze the input feature map into a compact global vector. We then split such vector into different groups or nodes and perform graph reasoning operation on such input node graphs. Finally, we reconstruct the original feature map by multiplying the reasoned vector back into the input feature. We specify the details of these three steps in the following parts. Fig 2 shows the detailed pipeline of our SR module.

Node squeezing It is well known that the global vector describes whole image statistics, which is a key component in many modern convolutional network architectures for different tasks such as object detection, scene parsing and image generation. The simplest way to calculate the global vector is the global average pooling, which calculates the first-order whole image statistics.

Recent works (Lin, RoyChowdhury, and Maji 2015; Chen et al. 2018b) use the bilinear pooling to capture second-order statistics of features and generate global representations. Compared with the conventional average and max pooling, which only computes first-order statistics, bilinear pooling can better capture and preserve complex relations. In particular, bilinear pooling gives a sum pooling of second-order features from the outer product of all the feature vector pairs $(\mathbf{b}_i, \mathbf{c}_i)$ within two input feature maps \mathbf{B} and \mathbf{C} . It can be expressed as follows:

$$\mathbf{G}_{bilinear}(\mathbf{B}, \mathbf{C}) = \mathbf{B}\mathbf{C}^T = \sum_{i=1}^{HW} \mathbf{b}_i \mathbf{c}_i^T, \quad (3)$$

where $\mathbf{B} = [\mathbf{b}_1, \dots, \mathbf{b}_i, \dots, \mathbf{b}_{HW}] \in \mathbb{R}^{C \times HW}$ and $\mathbf{C} = [\mathbf{c}_1, \dots, \mathbf{c}_i, \dots, \mathbf{c}_{HW}] \in \mathbb{R}^{C \times HW}$. The output size is $C \times C$.

To get a more compact vector for each node, in this paper, instead of generating outer product of all feature pairs from \mathbf{b}_i and \mathbf{c}_i within two input feature maps \mathbf{B} and \mathbf{C} , we calculate the Hadamard product:

$$\mathbf{G}_{global}(\mathbf{B}, \mathbf{C}) = \sum_{i=1}^{HW} \mathbf{b}_i \circ \mathbf{c}_i, \quad (4)$$

where \circ means the Hadamard product operation. To be note that, we first reduce channel dimension of input feature X by 1×1 convolution layer into \tilde{X} and then we perform pooling operation using Equ. 4 or simple global average pooling.

Node graph reasoning To form a node graph, we divide vector g into k different groups with each group size of d where $C = k \times d$. We use the graph convolution to model the relationship between nodes and consider it a fully-connected graph. As for the transformation \mathbf{W} in Equ. 1, we adopt a 1×1 convolutional layer to implement it. Moreover, for the adjacency matrix \mathbf{A} , we will show by experiments that our Squeeze Reasoning mechanism is not sensitive to these choices, indicating that the generic graph reasoning behavior is the main reason for the observed improvements. We will describe two specific choices in the following part:

Learned matrix. We follow the same settings in GloRe (Chen et al. 2019), a simple choice of \mathbf{A} is a 1×1

convolutional layer that can be updated by the general back-propagation. Similar to previous works (Li and Gupta 2018; Chen et al. 2019), we consider adopting the Laplacian matrix $(\mathbf{I} - \mathbf{A}_g)$ to propagate the node features over the graph, where the identity matrix \mathbf{I} serves as a residual sum connection. In this setting, the Graph Reasoning can be formulated as follows:

$$\mathbf{G}_{output} = \sigma(\mathbf{W}_g \mathbf{G}_{input} (\mathbf{I} - \mathbf{A}_g)), \quad (5)$$

where σ is the ReLU operation.

Correlation matrix. Another choice is to adopt the self-attention mechanism for information exchange (Wang et al. 2018b), by which the reasoning process can be written as follows:

$$\mathbf{G}_{output} = \sigma \{ \rho_g(\mathbf{G}_{input}) [\phi_g(\mathbf{G}_{input})^T \theta_g(\mathbf{G}_{input})] \}, \quad (6)$$

where ϕ_g , θ_g and ρ_g are three 1×1 convolutions. ϕ_g and θ_g are named ‘query’ and ‘key’, respectively. The ρ_g operation here, named ‘value’, functions the same as the \mathbf{W}_g in the ‘Learned matrix’ mechanism. The results generated by operations inside the $[\cdot]$ form the adjacency matrix \mathbf{A} . To be noted that, either reasoning process can be adopted in our framework and more detailed results can be referred to the experiment part.

Feature reconstruction The final step is to generate the representation \mathbf{R} . To reconstruct the feature map, we first reshape the reasoned vector and multiply it with $\tilde{\mathbf{X}}$ to high-light different channels according to the input scene where $\tilde{\mathbf{X}} = \mathbf{X} \mathbf{G}_{output}$. Then we adopt another 1×1 convolution layers \mathbf{W}_R to project the $\tilde{\mathbf{X}}$ into original shape. Following the same idea of residual learning (He et al. 2016; Wang et al. 2018b), we get the final output \mathbf{Y} by adding original input \mathbf{X} . Then the feature map can be reconstructed as follows:

$$\mathbf{Y} = \mathbf{W}_R \tilde{\mathbf{X}} + \mathbf{X} \quad (7)$$

where \mathbf{W}_R is a learnable linear transformation and \mathbf{Y} is the final output feature.

Analysis and discussion

Relationship with Previous Operators: Compared with the Non-local block (Wang et al. 2018b), instead of affinity modeling on pixel-level, our SR extends the reasoning on channel dimension, which captures statistics of whole feature map space. Compared with the SE block (Badrinarayanan, Kendall, and Cipolla 2017), our SR module captures more relational information and performs channel diffusion more efficiently than the fixed fully connected layers. Moreover, the experiment results show the advantages of our module.

Computation and memory analysis: Compared with previous self-attention methods (Wang et al. 2018b; Huang et al. 2018b; Chen et al. 2018b), we compare our module computation in Tab. 1 which shows our module is both lightweight on both computation and memory compared with previous methods. To be noted, we only consider the reasoning part in both computation cost and affinity memory. As shown in the last row, our module linearly depends

Methods	Computation	Affinity Memory
Non-local (Wang et al. 2018b)	$O(C(HW)^2)$	$O((HW)^2)$
A2Net (Chen et al. 2018b)	$O(C^2(HW))$	$O(C^2)$
CGNL (Yue et al. 2018)	$O(CHWP)$	$O(P^2)$
CCNet (Huang et al. 2018b)	$O(CHW(H+W))$	$O(HW(H+W))$
DANet (Fu et al. 2018)	$O(C(HW)^2 + HW(C)^2)$	$O((HW)^2 + (C)^2)$
SRNet	$O(CHW + C)$	$O(K^2 + M^2)$

Table 1: Time complexity comparison of non-local operations with our proposed SR module where H and W is spatial resolution and C is channel dimension. P is the order of Taylor expansion of kernel function in (Yue et al. 2018) and $KM = C/2$. Note that we ignore the channel reduction process since they are equal for computation cost.

on the input resolution in terms of computation and has no relation with the input resolution in terms of affinity memory. More analysis can be found in the experimental part.

Network architecture

The proposed SR module can be easily incorporated into the existing CNN architectures. We detail our network design in the task of semantic segmentation and instance level segmentation.

Semantic Segmentation: We adopt the Fully Convolution Networks (FCNs) (Long, Shelhamer, and Darrell 2015) as the backbone model. In particular, we choose ImageNet (Russakovsky et al. 2015) pretrained ResNet (He et al. 2016), remove the last two down-sampling operations and adopt the multi-grid (Yu and Koltun 2016) dilated convolutions. We remove the last two down-sampling operations and use the dilation convolutions instead to hold the feature maps from the last two stages $\frac{1}{8}$ of the input image. Concretely, all the feature maps in the last three stages have the same spatial size. Following the same setting (Huang et al. 2018b; Zhu et al. 2019b), we insert our proposed module between two 3×3 convolution layers (both layers output $D = 512$ channels), which are appended at the end of the FCN. Following (Zhao et al. 2017), our model has two supervisions: one after the final output of our model while another at the output layer of Stage4 as auxiliary cross-entropy loss. For real-time segmentation models, we choose DF-seg models (Li et al. 2019c) as a baseline and we replace their head with our SR module.

Instance level segmentation: For instance segmentation and panoptic segmentation, We choose two-stage mask-rcnn-like architectures (He et al. 2017; Kirillov et al. 2019a) We insert our module on the outputs of bottleneck in ResNet (He et al. 2016) layer4 for context modeling.

Experiment

We verify the proposed module on four scene understanding tasks, including semantic segmentation, object detection, instance segmentation, panoptic segmentation. Our method outperforms state-of-the-art methods on four benchmarks for semantic segmentation, including Cityscapes, ADE20K and Pascal Context, with much less computation cost. Experiments on the other three vision tasks also demonstrate the effectiveness of the proposed module. All the experiments are under the same setting for each task and each

Squeeze		Reasoning			mIoU (%)	$\Delta(\%)$
GAP	GHP	FC	GCN	SA		
-	-	-	-	-	74.8	-
✓	-	-	-	-	75.3	+0.5
-	✓	-	-	-	76.3	+1.5
✓	-	✓	-	-	76.6	+1.8
-	✓	✓	-	-	76.8	+2.0
✓	-	-	✓	-	79.1	+4.3
-	✓	-	✓	-	79.9	+5.1
-	✓	-	-	✓	79.5	+4.7

Table 2: Ablation study on the components of the proposed SR module. (a) Exploration on SR module design. **GHP**: Global Hadamard pooling. **FC**: Fully-connected layers. **GCN**: Reasoning with the graph convolution as Eq. 5. **SA**: Reasoning using the self-attention mechanism as Eq. 6.

dataset for a fair comparison. More detailed settings and analysis can be found in the supplementary file.

Experiments on semantic segmentation

Experimental settings: We first carry out detailed ablation studies and visual analysis on proposed approaches. Then we compare our method with previous works to show both efficiency and effectiveness on different benchmarks. We implement our method based on the PyTorch framework (Paszke et al. 2017). For the Cityscapes dataset, following the same settings in PSPNet(Zhao et al. 2017) where momentum and weight decay coefficients are set to 0.9 and $5e-4$ respectively, and “poly” learning rate schedule is used. For ablation studies, we choose ResNet-50 as the backbone. More details can be found in the supplementary file.

Ablation on SR framework design: We first present a detailed analysis of each component of SR through ablation study and report results in Tab. 2(a). Comparing with the baseline, all SR versions equipped with different components achieve considerable improvements. By switching different squeezing operations, we find Global Hadamard Pooling (GHP) performs consistently better than Global Average Pooling (GAP) across differently used reasoning methods. Moreover, reasoning with Graph Convolutional Network and Self-Attention brings more improvements, even comparing with methods using global information from squeezing operation and further transformed by fully-connected layers(FC). Our segmentation models are trained under the best setting in this table.

Ablation on hyper-parameter settings: To select the best hyper-parameter K , we also carry out an ablation study on the number of groups. To control independent variables, we fix $KM = C/2$, and only adjust K . We also explore the effect of channel reduction ratio with fixed K . The results are shown in Fig 3. From which, we can see that the selection of K doesn’t influence too much while reducing channel leads to inferior results. We set $K = 16$ and ratio to 2 as default for the remaining experiments.

Comparisons with context aggregation approaches: In Tab. 3, we compare the performance of different context aggregation approaches, where SR achieves the best mIoU with ResNet-50 as the backbone. We give detailed and fair comparisons in terms of flops, parameters and memory cost. In particular, SR performs even better than all the non-local methods (Huang et al. 2018b; Wang et al. 2018b; Yue et al.

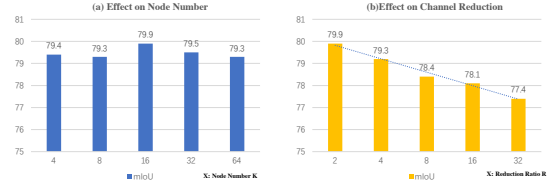


Figure 3: Ablation on hyper-parameter settings. (a) Effect on node number. (b) Effect on channel reduction.

Method	mIoU (%)	FLOPS	Params	Mem
dilated FCN	74.8	241.05G	23.63M	3249M
+ASPP (Chen et al. 2017)	77.4	+148.37G	+15.54M	+191.20M
+PSP (Zhao et al. 2017)	77.2	+174.09G	+23.07M	+221.05M
$+2 * 3 \times 3$	-	+108.74G	+11.80M	+108.00M
+SE (Hu, Shen, and Sun 2018)	74.6	9.47M ↑	0.03M ↑	18.88M ↑
+NL (Wang et al. 2018b)	78.0	48.36G↑	0.53M↑	865.52M↑
+A2Net (Chen et al. 2018b)	78.1	4.94G↑	0.53M↑	183.32M↑
+CGNL (Yue et al. 2018)	78.2	4.91G↑	0.53M↑	201.94M↑
+RCCA (Huang et al. 2018b)	78.5	11.55G↑	0.53M↑	394.28M↑
+EMAU (Li et al. 2019b)	77.9	6.97G↑	0.54M↑	132.64M↑
+SR (GAP)	79.1	2.43G↑	0.26M↑	82.31M↑
+SR (GHP)	79.9	3.64G↑	0.40M↑	110.75M↑

Table 3: Comparison experiments using different context modeling methods on the Cityscapes validation set, where dilated FCN (ResNet-50) serves as the baseline method. The FLOPS and the Memory (Mem) are computed over the input image of size $768 \times 768 \times 3$ and input feature map of size $96 \times 96 \times 2048$. For models other than ASPP and PSP, the overhead of the 3×3 convolutions before and behind the modules are shown separately as the row $+2 * 3 \times 3$. ↑ means the relative overheads over those of $+2 * 3 \times 3$. All the methods are evaluated under the same setting for the fair comparison.

2018), which aggregates long-range contextual information in a pixel-wise manner. This indicates the effectiveness of cross-channel relationships in building compact and better representations with fewer computation FLOPS. Fig 4(a) gives inference time comparison with different resolution image inputs on V100-GPU, which shows the advantages with high-resolution image inputs.

Visualization and analysis on learned node representation: Here, we give visualization analysis on different channel activation on the reasoned feature map. From Fig 5, we can see that each item corresponds to some abstract conceptions in the image. For example, the third-row item attends on the trucks and the cars while the second column shows that items focus on the stuff and background, and the fourth column items in group-10 are more sensitive to the small objects like poles and boundaries.

Visualization on predictions and feature maps: Fig. 6(a) compares segmentation results with and without reasoning. Without reasoning, pixels of large objects such as trucks and buses are often misclassified into similar categories due to ambiguities caused by limited receptive fields. The reasoning module resolves the above issue and delivers more consistent segmentation inside objects. Fig. 6(b) further investigates the effects of SR by directly comparing its input

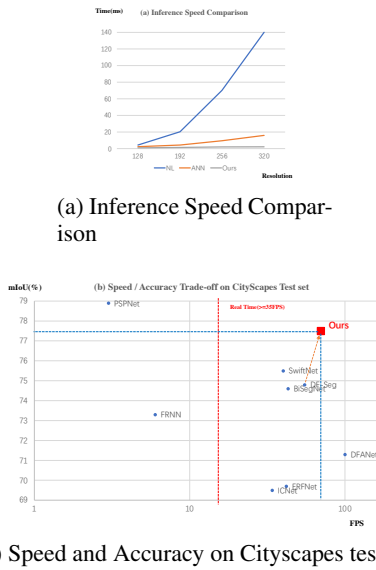


Figure 4: Efficiency analysis. (a) Speed Comparison with Non-local and its variants. (b) Speed and Accuracy trade-off on Cityscapes Test Set. Best view it in color and zoom in.

and output feature maps, where SR significantly improves the consistency of features inside objects, which is also the reason for consistent semantic map prediction. After SR, the features inner the objects have similar color and clearer boundaries shown the second column in Fig 6(b).

Comparisons with real time models: To further prove the efficiency of our module, we replace PPM head (Zhao et al. 2017) in DF-Seg-v2 (Li et al. 2019c) with our module. We set a new record on **best speed and accuracy trade-off** in Cityscapes test set with 77.5 %mIoU and 70 FPS shown in Fig. 4(b), which indicates the practical usage of our method. More detailed information can be found in the supplementary file.

Comparisons with state-of-the-art methods: In this section, we compare our method with state-of-the-art methods on four semantic segmentation benchmarks. Without bells and whistles, our method outperforms state-of-the-art models while costing less computation.

Results on Cityscapes: We train our model for 120K iterations using only the finely annotated data (trainval set), online hard negative mining is used following (Fu et al. 2018). Multi-scale and horizontal flip testing is used as previous works (Huang et al. 2018b). Tab. 4(a) compares the results, where our methods achieves **82.2%** mIoU and outperforms all previous state-of-the-art models by a large margin. In particular, our method is 0.7% mIoU higher than DANet (Fu et al. 2018), which uses non-local-like operator and is much efficient in both computation and memory cost due to the design of squeeze and reasoning. Our ResNet-50 based model achieves 81.0% mIoU and outperforms DenseASPP (Yang et al. 2018) by 0.4% with much larger backbone (Huang et al. 2017), which shows the effectiveness of our method. After replacing stronger backbone Wider-ResNet (Wu, Shen, and van den Hengel 2016), we

Method	Backbone	mIoU (%)
DFN (Yu et al. 2018b)	ResNet-101	79.3
CFNet (Zhang et al. 2019)	ResNet-101	79.6
DenseASPP (Yang et al. 2018)	DenseNet-161	80.6
GloreNet (Chen et al. 2018c)	ResNet-101	80.9
BAFPNet (Ding et al. 2019)	ResNet-101	81.4
CCNet (Huang et al. 2018b)	ResNet-101	81.4
ANNet (Zhu et al. 2019b)	ResNet-101	81.3
DANet (Fu et al. 2018)	ResNet-101	81.5
OCRNet (Yuan, Chen, and Wang 2020)	ResNet-101	81.8
SRNet	ResNet-50	81.0
SRNet	ResNet-101	82.2
SRNet	Wider-ResNet	83.3

(a) Results on the Cityscapes test set. All methods use only finely annotated data.

Method	Backbone	mIoU (%)
EncNet (Zhang et al. 2018a)	ResNet-50	49.2
DANet (Fu et al. 2018)	ResNet-50	50.1
SRNet	ResNet-50	50.8
EncNet (Zhang et al. 2018a)	ResNet-101	51.7
Ding et al. (Ding et al. 2018)	ResNet-101	51.6
DANet (Fu et al. 2018)	ResNet-101	52.6
SGR (Liang et al. 2018)	ResNet-101	52.5
ANNet (Zhu et al. 2019b)	ResNet-101	52.8
BAFPNet (Ding et al. 2019)	ResNet-101	53.6
EMANet (Li et al. 2019b)	ResNet-101	53.1
SRNet	ResNet-101	54.7

(b) Results on Pascal Context dataset.

Method	Backbone	mIoU (%)
PSPNet (Zhao et al. 2017)	ResNet-50	42.78
PSANet (Zhao et al. 2018b)	ResNet-50	42.97
UperNet (Xiao et al. 2018)	ResNet-50	41.55
EncNet (Zhang et al. 2018a)	ResNet-50	41.11
GCUNet (Li and Gupta 2018)	ResNet-50	42.60
SRNet	ResNet-50	43.42
PSPNet (Zhao et al. 2017)	ResNet-101	43.29
PSANet (Zhao et al. 2018b)	ResNet-101	43.77
SAC (Zhang et al. 2017)	ResNet-101	44.30
EncNet (Zhang et al. 2018a)	ResNet-101	44.65
GCUNet (Li and Gupta 2018)	ResNet-101	44.81
ANNet (Zhu et al. 2019b)	ResNet-101	45.24
SRNet	ResNet-101	45.53

(c) Results on the ADE20K dataset.

Table 4: Comparison with the state-of-the-art methods on Cityscapes, ADE20k and Pascal Context.

achieve **83.3 %mIoU** with **only** fine annotated data, which outperforms previous state-of-the-art methods by a large margin.

Results on Pascal Context: Tab. 4(b) reports results on Pascal Context. With ResNet-101 as the backbone, our method achieves 54.7% in mIoU with multi-scale inference, surpassing state-of-the-art alternatives by a large margin. Additionally, using the ResNet-50 backbone, we achieve 50.8% mIoU, which also outperforms the previous work (Fu et al. 2018) under the same setting.

Results on ADE20K: We also apply our method on ADE20K, which is challenging due to various image sizes, more semantic categories and a larger gap between training and validation set. Both results on ResNet-50 and ResNet-101 are reported. As shown in Tab. 4(c), Our method with ResNet-101 achieves the best results and comparable results with ResNet-50 backbone.

Results on MS COCO

To verify our module’s generality, we further conduct experiments on MS COCO (Lin et al. 2014) for more tasks, including object detection, instance segmentation and panoptic segmentation. For the first two tasks, our model is based

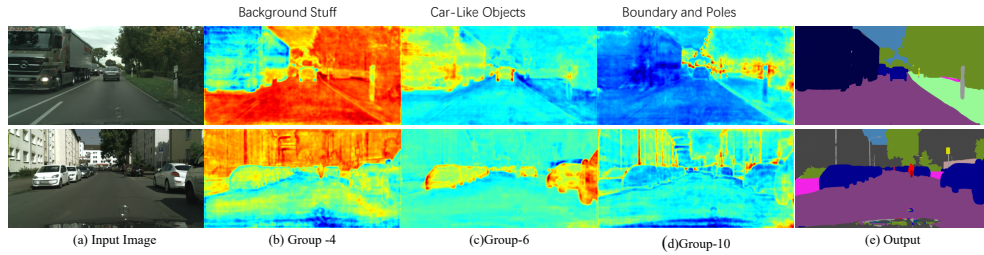
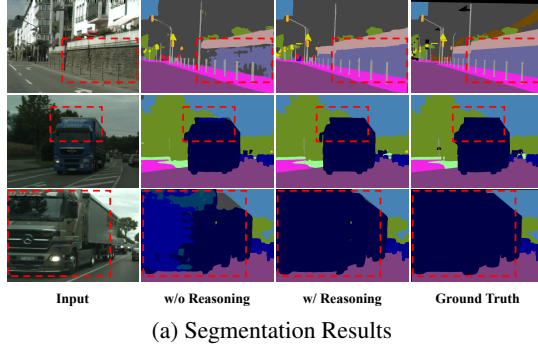
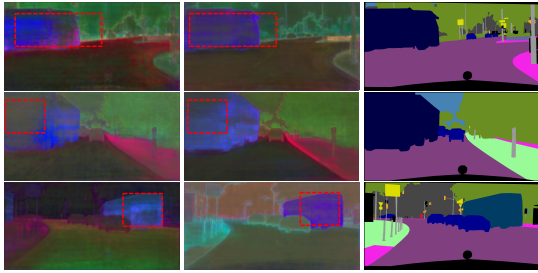


Figure 5: Visualization on learned group representation. We select the most salient channel from each node group. Such items capture specific concepts in the images. Best view in color and zoom in.



(a) Segmentation Results



(b) Feature Visualization

Figure 6: (a) Comparison of our results from cropped images where dilated-FCN with GAP- Squeeze operation as the baseline model. (b) The input and the output feature maps of the SR module. They are projected from 512-d to 3-d by PCA. Best view it in color and zoom in.

on the state-of-the-art method Mask R-CNN (He et al. 2017) and its variants (Cai and Vasconcelos 2018; Dai et al. 2017). For panoptic segmentation, we choose Panoptic FPN as our baseline (Kirillov et al. 2019a). We use open-source tools (Chen et al. 2018) to carry out all the experiments and report results on the MS COCO validation dataset. The GFlops are measured with 1200×800 inputs.

Results on object detection and instance segmentation: Tab. 5(a) compares results of both object detection and instance segmentation with various backbone networks (Xie et al. 2017) and advanced method (Cai and Vasconcelos 2018), where our method achieves consistently better performance on all backbones with less computation cost.

Results on panoptic segmentation: Panoptic Segmentation (Kirillov et al. 2019b) uses the PQ metric to capture

Backbone	Detector	AP-box	AP-mask	GFlops
R-50	Mask-RCNN	37.2	33.8	275.58
R-50	+NL (Wang et al. 2018b)	38.0	34.7	+30.5
R-50	+SR	38.4	34.9	+0.56
R-101	Mask-RCNN	39.8	36.0	351.65
R-101	+NL	40.5	36.7	+45.7
R-101	+SR	40.8	36.9	+1.32
X-101	Mask-RCNN	41.2	37.3	355.37
X-101	+SR	42.0	37.8	+1.32
X-101	Cascaded-Mask-RCNN	44.7	38.3	519.90
X-101	+SR	45.5	39.0	+1.32

(a) Experiments on COCO Object Detection and Instance Segmentation.

Method	Backbone	PQ	PQ (things)	PQ (stuff)	GFlops
Base	ResNet-50	39.0	45.9	28.7	270.8
+NL	ResNet-50	39.8	46.8	28.9	+30.5
+SR	ResNet-50	40.3	47.2	29.9	+0.56
Base	ResNet-101	40.3	47.5	29.5	346.87
+NL	ResNet-101	40.8	48.5	30.4	+45.7
+SR	ResNet-101	41.8	48.7	31.3	+1.32

(b) Experiments on COCO Panoptic Segmentation.

Table 5: Experiments on COCO dataset. (a) Detection results on the COCO 2017 validation set. **R-50**: ResNet-50. **R-101**: ResNet-101. **X-101**: ResNeXt-101 (Xie et al. 2017). (b) Panoptic segmentation results on the COCO 2017 validation set.

the performance for all classes (stuff and things) in a unified way. The results are shown in Tab. 5(b). Our method improves baseline and outperforms the non-local based methods through both overall evaluation and evaluations separated into thing and stuff, and the improvements are across both backbone, ResNet-50 and ResNet-101 with less computation cost.

Conclusion

This paper proposes a novel Squeezing and Reasoning framework for highly efficient deep feature representation learning for the scene understanding tasks. It learns to squeeze the feature to a node graph space where each node represents an abstract semantic concept while both memory and computation costs are significantly reduced. Extensive experiments demonstrate that our method can establish new state-of-the-arts on semantic segmentation while keeping efficiency. It also shows consistent improvement with respect to strong baselines over instance segmentation and panoptic segmentation with much less computation.

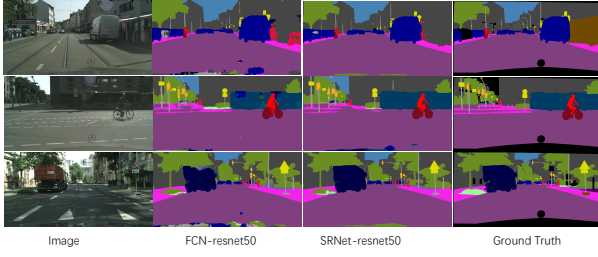


Figure 7: More qualitative results on Cityscapes validation set. Best viewed in color and zoom in.

Acknowledgement

We gratefully acknowledge the support of SenseTime Research for providing the computing resources. Z. Lin is supported by NSF China (grant no.s 61625301 and 61731018) and Major Scientific Research Project of Zhejiang Lab (grant no.s 2019KB0AC01 and 2019KB0AB02).

Supplementary Material

In this supplementary part, we report additional qualitative results of our approach, additional details about the experiment setting, more experiment results, and also additional experiments on Camvid (Brostow, Fauqueur, and Cipolla 2008).

Semantic segmentation experiments

Cityscapes (regular settings): This dataset (Cordts et al. 2016) is a benchmark that densely annotated for 19 categories in urban scenes. It contains 5000 fine annotated images in total and is divided into 2975, 500, and 1525 images for training, validation and testing, respectively. Images of this data are all with the same high resolution, i.e., 1024×2048 . It also provides 20000 coarsely annotated images. 30 classes are annotated and 19 of them are used for pixel-level semantic labeling tasks. We **do not** use the coarsely annotated set. For the final submission to the test server, we first train our model with 10k iterations, and then we fix the batch normalization layer to finetune for 2k more iterations. We use multi-scale inference with flip operation and the scales are $\{0.5, 0.75, 1, 1.25, 1.5, 2.0\}$ following DANet (Fu et al. 2018). The detailed results are shown in Tab. 7 where we report the models using ResNet-101 as the backbone. We give more visual examples on Cityscapes validation dataset shown in Fig 7. Compared with FCN baseline, our method can well handle the inner inconsistency problems of large objects.

Cityscapes (real-time settings): We mainly follow the DFANet (Li et al. 2019a). The networks with SR head are trained with the same setting, where stochastic gradient descent (SGD) with batch size of 16 is used as optimizer, with momentum of 0.9 and weight decay of $5e-4$. All models are trained for 50K iterations with an initial learning rate of 0.01. As a common practice, the “poly” learning rate policy is adopted to decay the initial learning rate by multiplying $(1 - \frac{\text{iter}}{\text{total_iter}})^{0.9}$ during training. Data augmentation

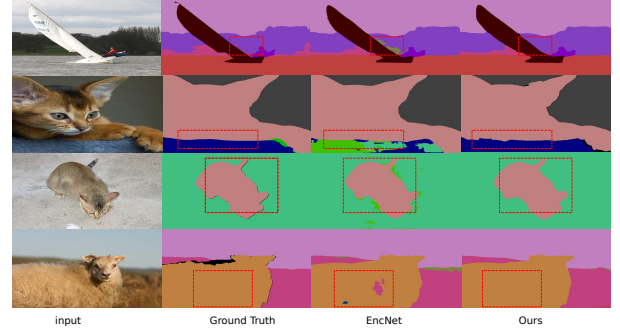


Figure 8: Comparison of our results on Pascal Context to the state-of-the-art EncNet (Zhang et al. 2018b). Note that our results are more consistent and have fewer artifacts. Best view in color and zoom in.

Method	InputSize	mIoU (%)	#FPS	#Params
ESPNet (Mehta et al. 2018)	512×1024	60.3	132	0.4M
ESPNetv2 (Mehta et al. 2019)	512×1024	62.1	80	0.8M
ERFNet (Romera et al. 2018)	512×1024	69.7	41.9	-
BiSeNet(ResNet-18) (Yu et al. 2018a)	768×1536	74.6	43	12.9M
BiSeNet(Xception-39) (Yu et al. 2018a)	768×1536	68.4	72	5.8M
ICNet (Zhao et al. 2018a)	1024×2048	69.5	34	26.5M
DFv1 (Li et al. 2019c)	1024×2048	73.0	80	9.37M
SwiftNet (Orsic et al. 2019)	1024×2048	75.5	39.9	11.80M
SwiftNet-ens (Orsic et al. 2019)	1024×2048	76.5	18.4	24.7M
DFANet (Li et al. 2019a)	1024×1024	71.3	100	7.8M
CellNet (Nekrasov et al. 2019)	768×1536	70.5	108	-
DFv2(baseline) (Li et al. 2019c)	1024×2048	74.8	55	18.83M
SRNet(DFv2)	1024×2048	77.5	65	18.87M

Table 6: Comparison on Cityscapes *test* set with state-of-the-art real-time models. For fair comparison, input size is also considered, and all models use single scale inference.

contains random horizontal flip, random resizing with scale range of $[0.75, 2.0]$, and random cropping with crop size of 1024×1024 . During inference, we use the whole picture as input to report performance. Tab 6 shows the results of our real-time model. Compared with previous real time models, our method achieves best speed and accuracy trade-off. Compared with baseline DFSeg (Li et al. 2019c), Our method has similar parameters but with more accurate and faster speed.

PASCAL Context (Mottaghi et al. 2014): This dataset provides detailed semantic labels for the whole scenes(Mottaghi et al. 2014). It contains 4998 images for training and 5105 images for validation. We train the network for 100 epochs with a batch size of 16, a crop size of 480. For evaluation, we perform multi-scale testing with the flip operation, which boosts the results for about 1.2% in mIoU. Fig. 8 shows the results of our method and EncNet. Compared with EncNet (Zhang et al. 2018b), our method achieves better consistent results on the object inner parts, benefited from better reasoned features.

ADE20K (Zhou et al. 2016): This is a more challenging scene parsing dataset annotated with 150 classes, which it contains 20k and 2k images for training and validation, respectively. We train the network for 120 epochs with a batch size of 16, a crop size of 512 and an initial learning rate

Method	road	swalk	build	wall	fence	pole	tlight	sign	veg.	terrain	sky	person	rider	car	truck	bus	train	mbike	bike	mIoU
DUC-HDC (Wang et al. 2018a)	98.5	85.5	92.8	58.6	55.5	65.0	73.5	77.8	93.2	72.0	95.2	84.8	68.5	95.4	70.9	78.7	68.7	65.9	73.8	77.6
ResNet38 (Wu, Shen, and van den Hengel 2016)	98.5	85.7	93.0	55.5	59.1	67.1	74.8	78.7	93.7	72.6	95.5	86.6	69.2	95.7	64.5	78.8	74.1	69.0	76.7	78.4
PSPNet (Zhao et al. 2017)	98.6	86.2	92.9	50.8	58.8	64.0	75.6	79.0	93.4	72.3	95.4	86.5	71.3	95.9	68.2	79.5	73.8	69.5	77.2	78.4
AAF (Ke et al. 2018)	98.5	85.6	93.0	53.8	58.9	65.9	75.0	78.4	93.7	72.4	95.6	86.4	70.5	95.9	73.9	82.7	76.9	68.7	76.4	79.1
SegModel (Falong Shen and Zeng 2017)	98.6	86.4	92.8	52.4	59.7	59.6	72.5	78.3	93.3	72.8	95.5	85.4	70.1	95.6	75.4	84.1	75.1	68.7	75.0	78.5
DFN (Yu et al. 2018b)	-	-	-	-	-	-	-	-	-	-	-	-	-	-	-	-	-	-	-	79.3
BiSeNet (Yu et al. 2018a)	-	-	-	-	-	-	-	-	-	-	-	-	-	-	-	-	-	-	-	78.9
PSANet (Zhao et al. 2018b)	-	-	-	-	-	-	-	-	-	-	-	-	-	-	-	-	-	-	-	80.1
DenseASPP (Yang et al. 2018)	98.7	87.1	93.4	60.7	62.7	65.6	74.6	78.5	93.6	72.5	95.4	86.2	71.9	96.0	78.0	90.3	80.7	69.7	76.8	80.6
BFPNet (Ding et al. 2019)	98.7	87.1	93.5	59.8	63.4	68.9	76.8	80.9	93.7	72.8	95.5	87.0	72.1	96.0	77.6	89.0	86.9	69.2	77.6	81.4
DANet (Fu et al. 2018)	98.6	87.1	93.5	56.1	63.3	69.7	77.3	81.3	93.9	72.9	95.7	87.3	72.9	96.2	76.8	89.4	86.5	72.2	78.2	81.5
SRNet(ss)	98.7	86.7	93.5	60.9	61.7	68.3	76.6	79.9	93.7	72.4	95.8	86.9	72.3	96.1	76.1	87.2	88.2	70.3	77.5	81.2
SRNet	98.8	88.0	93.9	64.6	63.3	71.5	78.9	81.8	93.9	73.7	95.8	87.9	74.5	96.4	72.4	88.2	86.2	72.0	79.0	82.2

Table 7: Per-category results on the Cityscapes test set compared with accurate models. Note that all the models are trained with only fine annotated data. Our method with ResNet101 backbone outperforms existing approaches on **15** out of 19 categories, and achieves **82.2%** mIoU.

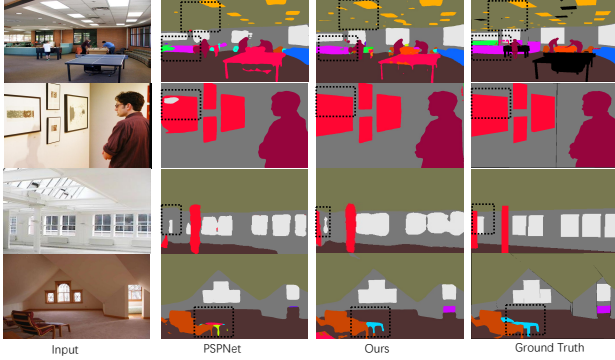


Figure 9: Comparison of our results with the state-of-the-art PSPNet (Zhao et al. 2017) method on the ADE-20k dataset. The black boxes show that our method can get more consistent results and missing objects. Best view in color and zoom in.

of $1e-2$. We perform multi-scale testing with the flip operation as the common setting in (Zhao et al. 2017). The visible results are shown in Fig. 9. Compared to PSPNet (Zhao et al. 2017), our method better handles inconsistent results and missing objects in the scene.

Camvid (Brostow, Fauqueur, and Cipolla 2008) is another road driving dataset. Camvid involves 367 training images, 101 validation images and 233 testing images with resolution of 960×720 . We use a crop size of 640 and training with 100 epochs. The results are shown in Tab 8. We report results with ResNet-50 and ResNet-101 backbone. With ResNet-101 as backbone, our method achieves **78.3%** mIoU, outperforming the state-of-the-art approach (Chandra, Couprie, and Kokkinos 2018) by a large margin (3.1%).

Experiments on COCO (Lin et al. 2014)

Training setting: Our models and all baselines are trained with the typical '1x' training schedule and setting from the public mmdetection (Chen et al. 2018) for all experiments on COCO. We do not embed the reconstruction loss during the training.

Qualitative results: Fig 10 shows the qualitative results on COCO validation set. The first two rows show our SR module can handle small missing objects (red boxes) while the

Method	Backbone	mIoU (%)
SegNet (Badrinarayanan, Kendall, and Cipolla 2017)	VGG-16	60.1
RTA (Huang et al. 2018a)	VGG-16	62.5
BiSeg (Yu et al. 2018a)	ResNet-18	68.7
PSPNet (Zhao et al. 2017)	ResNet-50	69.1
SRNet	ResNet-50	74.3
DilatedNet (Yu and Koltun 2016)	ResNet101	65.3
Dense-Decoder (Bilinski and Prisacariu 2018)	ResNext-101	70.9
BFP (Ding et al. 2019)	ResNet101	74.1
VideoGCRF (Chandra, Couprie, and Kokkinos 2018)	ResNet101	75.2
SRNet	ResNet-101	78.3

Results on the CamVid test set.

Table 8: Comparison with the state-of-the-art methods on CamVid datasets.

last two rows show our method can also avoid false positives (blue boxes) in the scene.

References

- Badrinarayanan, V.; Kendall, A.; and Cipolla, R. 2017. SegNet: A Deep Convolutional Encoder-Decoder Architecture for Image Segmentation. *TPAMI*.
- Bello, I.; Zoph, B.; Vaswani, A.; Shlens, J.; and Le, Q. V. 2019. Attention Augmented Convolutional Networks. In *ICCV*.
- Bilinski, P.; and Prisacariu, V. 2018. Dense Decoder Shortcut Connections for Single-Pass Semantic Segmentation. In *CVPR*.
- Brostow, G. J.; Fauqueur, J.; and Cipolla, R. 2008. Semantic Object Classes in Video: A High-Definition Ground Truth Database. *Pattern Recognition Letters* xx(x): xx-xx.
- Cai, Z.; and Vasconcelos, N. 2018. Cascade R-CNN: Delving Into High Quality Object Detection. In *CVPR*.
- Chandra, S.; Couprie, C.; and Kokkinos, I. 2018. Deep Spatio-Temporal Random Fields for Efficient Video Segmentation. In *The IEEE Conference on Computer Vision and Pattern Recognition (CVPR)*.
- Chen, K.; Pang, J.; Wang, J.; Xiong, Y.; Li, X.; Sun, S.; Feng, W.; Liu, Z.; Shi, J.; Ouyang, W.; Loy, C. C.; and Lin, D. 2018. mmdetection. <https://github.com/open-mmlab/mmdetection>.
- Chen, L.-C.; Papandreou, G.; Kokkinos, I.; Murphy, K.; and Yuille, A. L. 2015. Semantic Image Segmentation with Deep Convolutional Nets and Fully Connected CRFs. In *ICLR*.
- Chen, L.-C.; Papandreou, G.; Kokkinos, I.; Murphy, K.; and Yuille, A. L. 2018. DeepLab: Semantic Image Segmentation with Deep Convolutional Nets, Atrous Convolution, and Fully Connected CRFs. *TPAMI*.



(a) mask-rcnn-baseline

(b) + SR

Figure 10: Comparison of our results on COCO with Mask-RCNN with ResNet101 backbone. Best view in color and zoom in.

Chen, L.-C.; Papandreou, G.; Schroff, F.; and Adam, H. 2017. Rethinking Atrous Convolution for Semantic Image Segmentation. *arXiv preprint arXiv:1706.05587*.

Chen, L.-C.; Zhu, Y.; Papandreou, G.; Schroff, F.; and Adam, H. 2018a. Encoder-Decoder with Atrous Separable Convolution for Semantic Image Segmentation. In *ECCV*.

Chen, Y.; Kalantidis, Y.; Li, J.; Yan, S.; and Feng, J. 2018b. A²-Nets: Double Attention Networks. In *NIPS*.

Chen, Y.; Rohrbach, M.; Yan, Z.; Shuicheng, Y.; Feng, J.; and Kalantidis, Y. 2019. Graph-Based Global Reasoning Networks. In *CVPR*.

Chen, Y.; Rohrbach, M.; Yan, Z.; Yan, S.; Feng, J.; and Kalantidis, Y. 2018c. Graph-Based Global Reasoning Networks. *arXiv preprint arXiv:1811.12814*.

Cordts, M.; Omran, M.; Ramos, S.; Rehfeld, T.; Enzweiler, M.; Benenson, R.; Franke, U.; Roth, S.; and Schiele, B. 2016. The Cityscapes Dataset for Semantic Urban Scene Understanding. In *CVPR*.

Dai, J.; Qi, H.; Xiong, Y.; Li, Y.; Zhang, G.; Hu, H.; and Wei, Y. 2017. Deformable Convolutional Networks. In *ICCV*.

Ding, H.; Jiang, X.; Liu, A. Q.; Magnenat-Thalmann, N.; and Wang, G. 2019. Boundary-Aware Feature Propagation for Scene Segmentation. In *ICCV*.

Ding, H.; Jiang, X.; Shuai, B.; Qun Liu, A.; and Wang, G. 2018. Context Contrasted Feature and Gated Multi-Scale Aggregation for Scene Segmentation. In *CVPR*.

Falong Shen, Gan Rui, S. Y.; and Zeng, G. 2017. Semantic Segmentation via Structured Patch Prediction, Context CRF and Guidance CRF. In *CVPR*.

Fu, J.; Liu, J.; Tian, H.; Fang, Z.; and Lu, H. 2018. Dual attention network for scene segmentation. *arXiv preprint arXiv:1809.02983*.

He, J.; Deng, Z.; Zhou, L.; Wang, Y.; and Qiao, Y. 2019. Adaptive Pyramid Context Network for Semantic Segmentation. In *CVPR*.

He, K.; Gkioxari, G.; Dollár, P.; and Girshick, R. 2017. Mask r-cnn. In *ICCV*.

He, K.; Zhang, X.; Ren, S.; and Sun, J. 2016. Deep Residual Learning for Image Recognition. In *CVPR*.

Hu, J.; Shen, L.; and Sun, G. 2018. Squeeze-and-excitation networks. In *CVPR*.

Huang, G.; Liu, Z.; van der Maaten, L.; and Weinberger, K. Q. 2017. Densely Connected Convolutional Networks. In *CVPR*.

Huang, P.-Y.; Hsu, W.-T.; Chiu, C.-Y.; Wu, T.-F.; and Sun, M. 2018a. Efficient Uncertainty Estimation for Semantic Segmentation in Videos. In *The European Conference on Computer Vision (ECCV)*.

Huang, Z.; Wang, X.; Huang, L.; Huang, C.; Wei, Y.; and Liu, W. 2018b. Ccnet: Criss-cross attention for semantic segmentation. *arXiv preprint arXiv:1811.11721*.

Ke, T.-W.; Hwang, J.-J.; Liu, Z.; and Yu, S. X. 2018. Adaptive Affinity Fields for Semantic Segmentation. In *ECCV*.

Kipf, T. N.; and Welling, M. 2017. Semi-supervised classification with graph convolutional networks. In *ICLR*.

Kirillov, A.; Girshick, R.; He, K.; and Dollár, P. 2019a. Panoptic feature pyramid networks. In *CVPR*.

Kirillov, A.; He, K.; Girshick, R.; Rother, C.; and Dollar, P. 2019b. Panoptic Segmentation. In *CVPR*.

Li, H.; Xiong, P.; Fan, H.; and Sun, J. 2019a. DFANet: Deep Feature Aggregation for Real-Time Semantic Segmentation. In *CVPR*.

Li, X.; Zhong, Z.; Wu, J.; Yang, Y.; Lin, Z.; and Liu, H. 2019b. Expectation-Maximization Attention Networks for Semantic Segmentation. In *ICCV*.

Li, X.; Zhou, Y.; Pan, Z.; and Feng, J. 2019c. Partial Order Pruning: for Best Speed/Accuracy Trade-off in Neural Architecture Search. In *CVPR*.

Li, Y.; and Gupta, A. 2018. Beyond Grids: Learning Graph Representations for Visual Recognition. In *NIPS*.

Liang, X.; Hu, Z.; Zhang, H.; Lin, L.; and Xing, E. P. 2018. Symbolic Graph Reasoning Meets Convolutions. In *NIPS*.

Lin, T.-Y.; Maire, M.; Belongie, S.; Hays, J.; Perona, P.; Ramanan, D.; Dollár, P.; and Zitnick, C. L. 2014. Microsoft coco: Common objects in context. In *ECCV*.

Lin, T.-Y.; RoyChowdhury, A.; and Maji, S. 2015. Bilinear CNN Models for Fine-Grained Visual Recognition. In *ICCV*.

Long, J.; Shelhamer, E.; and Darrell, T. 2015. Fully convolutional networks for semantic segmentation. In *CVPR*.

Luo, W.; Li, Y.; Urtasun, R.; and Zemel, R. 2016. Understanding the effective receptive field in deep convolutional neural networks. In *NIPS*.

- Mehta, S.; Rastegari, M.; Caspi, A.; Shapiro, L.; and Hajishirzi, H. 2018. ESPNet: Efficient Spatial Pyramid of Dilated Convolutions for Semantic Segmentation. In *ECCV*.
- Mehta, S.; Rastegari, M.; Shapiro, L.; and Hajishirzi, H. 2019. ESPNetv2: A Light-Weight, Power Efficient, and General Purpose Convolutional Neural Network. In *CVPR*.
- Mottaghi, R.; Chen, X.; Liu, X.; Cho, N.-G.; Lee, S.-W.; Fidler, S.; Urtasun, R.; and Yuille, A. 2014. The Role of Context for Object Detection and Semantic Segmentation in the Wild. In *CVPR*.
- Nekrasov, V.; Chen, H.; Shen, C.; and Reid, I. 2019. Fast Neural Architecture Search of Compact Semantic Segmentation Models via Auxiliary Cells. In *CVPR*.
- Orsic, M.; Kreso, I.; Bevandic, P.; and Segvic, S. 2019. In Defense of Pre-Trained ImageNet Architectures for Real-Time Semantic Segmentation of Road-Driving Images. In *CVPR*.
- Paszke, A.; Gross, S.; Chintala, S.; Chanan, G.; Yang, E.; DeVito, Z.; Lin, Z.; Desmaison, A.; Antiga, L.; and Lerer, A. 2017. Automatic differentiation in PyTorch. In *NeurIPS workshops*.
- Ren, S.; He, K.; Girshick, R.; and Sun, J. 2015. Faster r-cnn: Towards real-time object detection with region proposal networks. In *NIPS*.
- Romera, E.; Alvarez, J. M.; Bergasa, L. M.; and Arroyo, R. 2018. ERFNet: Efficient Residual Factorized ConvNet for Real-Time Semantic Segmentation. *IEEE Trans. Intelligent Transportation Systems* 263–272.
- Russakovsky, O.; Deng, J.; Su, H.; Krause, J.; Satheesh, S.; Ma, S.; Huang, Z.; Karpathy, A.; Khosla, A.; Bernstein, M.; Berg, A. C.; and Fei-Fei, L. 2015. ImageNet Large Scale Visual Recognition Challenge. *IJCV*.
- Vaswani, A.; Shazeer, N.; Parmar, N.; Uszkoreit, J.; Jones, L.; Gomez, A. N.; Kaiser, Ł.; and Polosukhin, I. 2017. Attention is all you need. In *NIPS*.
- Wang, P.; Chen, P.; Yuan, Y.; Liu, D.; Huang, Z.; Hou, X.; and Cottrell, G. 2018a. Understanding Convolution for Semantic Segmentation. In *WACV*.
- Wang, X.; Girshick, R.; Gupta, A.; and He, K. 2018b. Non-Local Neural Networks. In *CVPR*.
- Wu, Z.; Shen, C.; and van den Hengel, A. 2016. Wider or Deeper: Revisiting the ResNet Model for Visual Recognition. *arXiv preprint arXiv:1611.10080*.
- Xiao, T.; Liu, Y.; Zhou, B.; Jiang, Y.; and Sun, J. 2018. Unified Perceptual Parsing for Scene Understanding. In *ECCV*.
- Xie, S.; Girshick, R.; Dollár, P.; Tu, Z.; and He, K. 2017. Aggregated residual transformations for deep neural networks. In *CVPR*.
- Yang, M.; Yu, K.; Zhang, C.; Li, Z.; and Yang, K. 2018. DenseASPP for Semantic Segmentation in Street Scenes. In *CVPR*.
- Yu, C.; Wang, J.; Peng, C.; Gao, C.; Yu, G.; and Sang, N. 2018a. BiSeNet: Bilateral Segmentation Network for Real-time Semantic Segmentation. In *ECCV*.
- Yu, C.; Wang, J.; Peng, C.; Gao, C.; Yu, G.; and Sang, N. 2018b. Learning a Discriminative Feature Network for Semantic Segmentation. In *CVPR*.
- Yu, F.; and Koltun, V. 2016. Multi-Scale Context Aggregation by Dilated Convolutions. In *ICLR*.
- Yuan, Y.; Chen, X.; and Wang, J. 2020. Object-Contextual Representations for Semantic Segmentation. *arXiv preprint arXiv:1909.11065*.
- Yue, K.; Sun, M.; Yuan, Y.; Zhou, F.; Ding, E.; and Xu, F. 2018. Compact generalized non-local network. In *NIPS*.
- Zhang, H.; Dana, K.; Shi, J.; Zhang, Z.; Wang, X.; Tyagi, A.; and Agrawal, A. 2018a. Context Encoding for Semantic Segmentation. In *CVPR*.
- Zhang, H.; Dana, K.; Shi, J.; Zhang, Z.; Wang, X.; Tyagi, A.; and Agrawal, A. 2018b. Context Encoding for Semantic Segmentation. In *CVPR*.
- Zhang, H.; Zhang, H.; Wang, C.; and Xie, J. 2019. Co-Occurrent Features in Semantic Segmentation. In *CVPR*.
- Zhang, R.; Tang, S.; Zhang, Y.; Li, J.; and Yan, S. 2017. Scale-adaptive convolutions for scene parsing. In *ICCV*.
- Zhao, H.; Qi, X.; Shen, X.; Shi, J.; and Jia, J. 2018a. ICNet for Real-Time Semantic Segmentation on High-Resolution Images. In *ECCV*.
- Zhao, H.; Shi, J.; Qi, X.; Wang, X.; and Jia, J. 2017. Pyramid Scene Parsing Network. In *CVPR*.
- Zhao, H.; Zhang, Y.; Liu, S.; Shi, J.; Change Loy, C.; Lin, D.; and Jia, J. 2018b. PSANet: Point-wise Spatial Attention Network for Scene Parsing. In *ECCV*.
- Zhou, B.; Zhao, H.; Puig, X.; Fidler, S.; Barriuso, A.; and Torralba, A. 2016. Semantic understanding of scenes through the ADE20K dataset. *arXiv preprint arXiv:1608.05442*.
- Zhu, X.; Hu, H.; Lin, S.; and Dai, J. 2019a. Deformable ConvNets V2: More Deformable, Better Results. In *CVPR*.
- Zhu, Z.; Xu, M.; Bai, S.; Huang, T.; and Bai, X. 2019b. Asymmetric Non-local Neural Networks for Semantic Segmentation. In *ICCV*.